IEEE Access
Multidisciplinary | Rapid Review | Open Access Journal

Received August 1, 2019, accepted August 21, 2019, date of publication September 2, 2019, date of current version September 13, 2019.

Digital Object Identifier 10.1109/ACCESS.2019.2938846

Analysis of Pre- and Post-Mine Closure Surface Deformations in Western Xuzhou Coalfield From 2006 to 2018

MEINAN ZHENG[1,2], HONGZHEN ZHANG[1,2], KAZHONG DENG[1,2], SEN DU[3], AND LIUYU WANG[1,2]

[1]Jiangsu Key Laboratory of Resources and Environmental Information Engineering, China University of Mining and Technology, Xuzhou 221116, China
[2]School of Environment Science and Spatial Informatics, China University of Mining and Technology, Xuzhou 221116, China
[3]The CommSensLab, Department of Signal Theory and Communications, Universitat Politècnica de Catalunya, 08034 Barcelona, Spain

Corresponding author: Hongzhen Zhang (hongyuhen@163.com)

This work was supported by the Outstanding Innovation Scholarship for Doctoral Candidate of "Double First Class" Construction Disciplines of CUMT.

ABSTRACT Economic development and population expansion in mining cities have led to a growing scarcity of land for construction and thus the closed mines land reuse is extremely urgent. Exploration of the law of surface deformation in closed mine is therefore significance for the development of mining cities. In this study, we first used the StaMSBAS technique to reveal surface deformation of western Xuzhou coalfield from 16/6/2006 to 19/8/2018, based on 77 SAR images. The result of ALOS-1 monitoring was validated by levelling data, and it was shown that the root-mean-square-error and standard deviation were 31.8 mm and 28.9 mm, respectively. The law of surface deformation that occurred before and after mine closure was finally analysed. It was found that: 1) After mine closure, the surface deformation of Jiahe mine experienced the process of subsidence, relative stability and then uplift, and the surface deformations of Zhangxiaolou and Pangzhuang mines changed from slow subsidence to accelerated subsidence. 2) Where the maximum pre-closure subsidence occurred at Jiahe mine, the residual subsidence and uplift that occurred after mine closure was also significant, the correlation coefficients were 0.62 and 0.65, respectively. When the mines were active, surface subsidence of Jiahe and Zhangxiaolou mines was positively correlated with the strike mining degree, with correlation coefficients of 0.90 and 0.83, respectively. After Jiahe mine closure, the residual subsidence was positively correlated with the strike mining degree, and the surface uplift was positively correlated with the depth-to-thickness ratio, the correlation coefficients were both 0.70.

INDEX TERMS Closed mine, InSAR, secondary deformation, groundwater.

I. INTRODUCTION

In China, adjustments to policy and the structural optimization of the coal sector have resulted in the closure of 7100 coal mines during the 12th Five Year Plan [1]. After mines closure, the environmental rehabilitation, transformation and development of closed mines have become important problems for the socioeconomic development of mining cities [2]. When the mine drainage equipment ceases operation, the groundwater level rises, which will alters the stress and bearing capacity of the broken rocks in goaf. This results in the surface secondary deformation, which threatens the safety of buildings that were constructed on top of the closed mines [3], [4]. The surface deformations that occur before and after mine closure are related to each other but are different. The surface deformation exhibit a form of continuity over time. When the mine is active, the extraction of underground minerals lead to surface deformation. After mines closure, the surface will continue to deform due to factors such as rising groundwater and inadequately compacted broken rocks in goaf. The surface deformation that occurs before and after mine closure are also spatially correlated. Since overburden fractures are most severe in locations where the surface deformation occurred in coal mining, these locations exhibit the most intense surface deformation (e.g. surface uplift and collapse) as groundwater level rise after the mine is closed. Moreover, the mechanism causing surface deformation occurring before and after mine closure differ. The deformation during mining is caused by

The associate editor coordinating the review of this article and approving it for publication was Krishna Kant Singh.

load-induced rheological and creep in the overburden after the removal of underground minerals. After mine closure, in addition to the load-induced deformation that still occur in the overburden, rising groundwater level will also alter the pore pressure in the rock strata, which change the effective stresses acting on the broken rocks in goaf and cause deformation. Acquiring the surface deformation that occur before and after mine closure is therefore important for determining the law of surface deformation, refining theories of mining subsidence, land-use planning, and stability evaluation for building above closed mines.

Traditional monitoring methods (such as levelling and global navigation satellite system) can provide point deformation with high accuracy. However, it is difficult to obtain the spatiotemporal development law of surface deformation due to its low spatial coverage and only point-like deformation [5]–[7]. After mine closure, due to the characteristics of surface deformation such as long-term and concealment, it will bring difficulties to the layout, preservation of observation stations and determination of the monitoring period.

Compared to traditional methods, differential interferometric synthetic aperture radar (DInSAR) is efficient, usable at all day in all weather conditions, and highly accurate [8], [9]. The DInSAR technique has already been applied in studies concerning earthquakes [10], volcanoes [11], urban groundwater loss and subsidence [12], infrastructures [13], archaeology and cultural heritage protection [14], and mines [15], [16]. SAR image is high resolution, wide coverage (Sentinel-1A/B Interferometric Wide (IW) mode can reach 250 km $\times$ 160 km), and has short revisit period (Sentinel-1A/B is only 6 days). Therefore, SAR image is excellent for exploration the location and scope of surface deformation in mining areas, both before and after mine closure. SAR archive image also has significant advantages in obtaining the surface deformation that has occurred in the mining areas. However, the DInSAR is severely affected by spatial and temporal decorrelation and atmospheric noise. As the surface deformation that occur after mine closure is small and sustained over a long period of time the accuracy of DInSAR monitoring can be limited.

Since Usai and Hanssen [17] proposed the acquisition of deformation using pixels that maintain high coherence over long time scales, various InSAR techniques have been suggested for the analysis of deformation over long period to overcome the weaknesses of the DInSAR technique. This includes single-master approaches such as the least-squares approach [18], [19], persistent scatterer InSAR (PSInSAR) [20], [21], interferometric point target analysis (IPTA) [22], and the coherent pixels technique (CPT) [23], as well as multi-master approaches such as the small baseline subset (SBAS) technique [24] and temporarily coherent point InSAR (TCPInSAR) [25], [26]. The PSInSAR surmounts the weaknesses of DInSAR by incorporating the recognition and analysis of coherent points. Although the PSInSAR can achieve millimeter-level accuracy in surface deformation monitoring, this approach requires a large amount of SAR images (more than 20 scenes). For the SBAS approach, decorrelation is suppressed through the selection of interferometric pairs with short temporal and spatial baselines. The SBAS technique requires a smaller number of SAR images than the PSInSAR, without compromising its accuracy in surface deformation monitoring, and performs very well in the detection of non-linear deformations. However, in non-urban areas with a lack of artificial constructions it can be difficult to select a sufficient number of coherent points for PSInSAR or SBAS analysis. This can result in excessively large distances between the coherent points, which makes phase unwrapping extremely difficult. To solve this problem, Hooper [27] proposed the Stanford Method for Persistent Scatterers (StaMPS) SBAS technique, where deformations are obtained through the identification of slowly decorrelating filtered phase (SDFP) pixels. Using this method it is possible to detect some surface deformations even in vegetated areas where there is a lack of coherent targets. Since the study area is densely vegetated, the StaMSBAS technique was used to detect the surface deformation.

II. STUDY DATA AND AREA

A. DATASETS

We collected a total of 77 SAR images. In particular, the 14 scenes of ascending ENVISAT image were acquired from 16/6 /2006 to 1/2/ 2008; the 9 scenes of ascending ALOS-1 image were acquired from 20/2/2007 to 16/1/2011; the 54 scenes of ascending Sentinel-1A image were acquired from 4/10/2016 to 19/8/2018. The images footprints are shown in Fig. 1(a), and the imaging parameters of different images are shown in Table 1. The terrain phase was eliminated by the Shuttle Radar Topography Mission (SRTM) digital elevation model (DEM) 3 arc second data provided by the NASA [28]. In order to improve the orbit accuracy of the ENVISAT image, the DORIS precise orbit data provided by the European Space Agency (ESA) were adopted.

B. WESTERN XUZHOU COALFIELD

The study area is located in the Tongshan and Quanshan districts of western Xuzhou, approximately 13 km from the centre of Xuzhou city. This area is a topographically flat and level alluvial plain that was formed by flooding of the Yellow River. The study area includes Cambrian, Ordovician, Carboniferous, Permian, and Quaternary strata. The primary coal-bearing strata are found within the Taiyuan Formation from the Upper Carboniferous, and the Shanxi and Lower Shihezi Formations that formed during the Lower Permian.

The study area includes the Jiahe mine, Pangzhuang mine, and the Zhangxiaolou mine, with an area of about 60.33 km^2. Due to decades of coal mining, large subsidence have occurred at the surface of the study area, which have subsequently filled with water to form ponds. The water depth of a subsidence area can reach up to 5 – 6 m. The water bodies at the surface of the mining field consist mainly of water-filled subsidence areas, as well as the Shixin River and Shitun River (shown in Fig. 1(b)). Blue water body as a

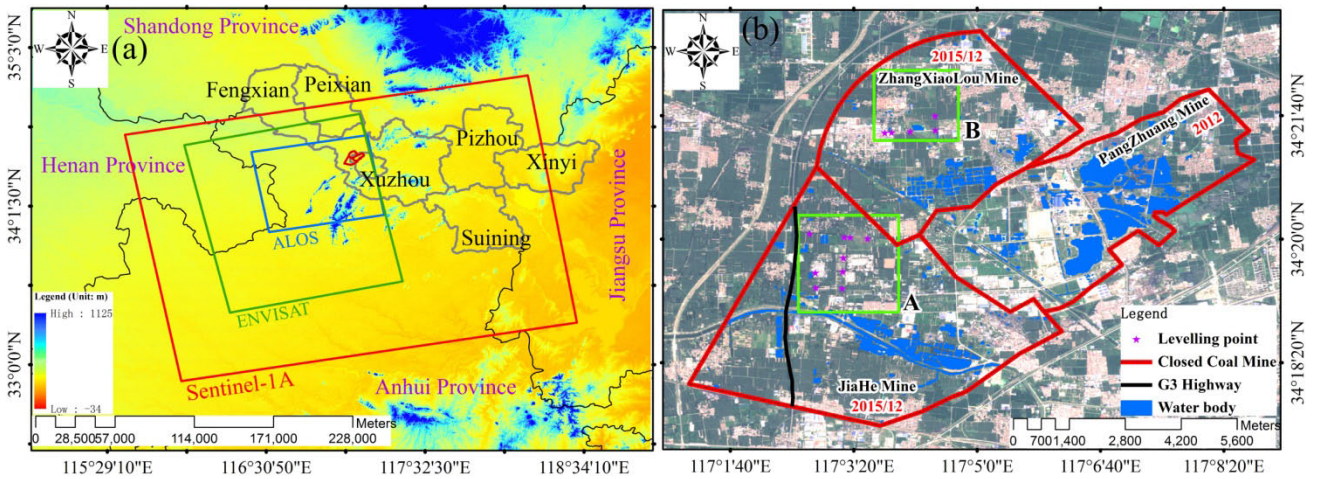

FIGURE 1. Overview of the study area. (a) Geographical location of the study area. The red, green and blue boxes are, respectively, the coverage range of the Sentinel-1A, ENVISAT and ALOS-1; The base map is SRTM DEM. (b) The spatial distribution of mines. The green rectangular (A and B) are the areas selected for the Discussion section; base map is Sentinel-2A optical image.

TABLE 1. Imaging parameters of SAR images.

	Incidence angle	Resolution(azimuth×range)	Repeat cycle	Wavelength/band	Polarization mode
ENVISAT	18.8°	3.92 m×7.80 m	35 days	0.056 m/C	VV
ALOS-1	38.7°	3.17 m×4.68 m	46 days	0.236 m/L	HH
Sentinel-1A	39.2°	13.94 m×2.33 m	12 days	0.056 m/C	VH

result of supervised classification of Landsat-8 optical image on 9/3/2018. The spatial distribution of mines and the mine closure date are reported on the Fig. 1(b).

III. METHOD

The coherent points selected by the StaMSBAS technique are known as SDFP points, the initial SDFP candidates are selected using the amplitude difference dispersion index ($D_{\Delta A}$). The $D_{\Delta A}$ threshold is often empirically defined as equal to 0.6 [29], [30]. The data processing flow is as follows:

Images acquired by ENVISAT, ALOS-1, and Sentinel-1A on 16/2/2007, 10/1/2009, and 22/12/2017 were selected as master images; the slave images were then registered and resampled with respect to these masters. To minimise the effects of spatial and temporal decorrelation, the maximum temporal and perpendicular baselines for the ENVISAT, ALOS-1, and Sentinel-1A data were set at 106 days, 369days, 37days and 900 m, 4000m, 150m respectively, 179 interferometric pairs were created by GAMMA software (as shown in Fig. 2). To reduce the effects from noise and to increase coherence, multi-look processing was performed on the ENVISAT, ALOS-1, and Sentinel-1A images, which produced pixels of approximately 24 m, 7 m, 20 m, respectively.

Assuming M SAR images were used to form N ($(M-1) \leq N \leq M*(M-1)/2$) interferometric pairs. The candidate SDFP (SDFPc) points were then determined according to the $D_{\Delta A}$ of the pixels. After the flat-earth and topographic phases of the SDFPc points were removed, the interferometric phase of the x-th SDFPc in the i-th interferogram ($\varphi_{x,i}$) is expressed as:

$$\varphi_{x,i} = w\left\{\emptyset_{D,x,i} + \emptyset_{A,x,i} + \Delta\emptyset_{Orb,x,i} + \Delta\emptyset_{\theta,x,i} + \emptyset_{N,x,i}\right\} \quad (1)$$

where w $\{\cdot\}$ is the wrapping operator. $\emptyset_{D,x,i}$, $\emptyset_{A,x,i}$ and $\Delta\emptyset_{Orb,x,i}$ are the deformation phase, atmospheric phase and orbit error phase, respectively, which are strongly spatially correlated. $\Delta\emptyset_{\theta,x,i}$ is the look error phase caused by terrain errors and the difference between strong scatterers and pixel centres, which is partially spatially correlated [29]. $\emptyset_{N,x,i}$ is the noise phase, which has a random spatiotemporal distribution.

The spatially correlated phases in (1) can be estimated using an adaptive bandpass filter. After the spatially correlated phase ($\tilde{\varphi}_{x,i}$) has been estimated, it can be removed from (1):

$$\varphi_{x,i} - \tilde{\varphi}_{x,i} = w\left\{\Delta\emptyset^{u}_{\theta,x,i} + \emptyset^{u}_{N,x,i} + \delta_{x,i}\right\} \quad (2)$$

where u superscript indicates that the term is spatially uncorrelated. Since deformation phase, atmospheric phase, and orbit error phase are strongly spatially correlated, the value of δ is very small. The spatially uncorrelated look error ($\Delta\emptyset^{u}_{\theta,x,i}$) is linearly related to the perpendicular baseline ($B_{\perp,x,i}$), such that:

$$\Delta\emptyset^{u}_{\theta,x,i} = \frac{4\pi}{\lambda} B_{\perp,x,i} \Delta\theta^{u}_{x} \quad (3)$$

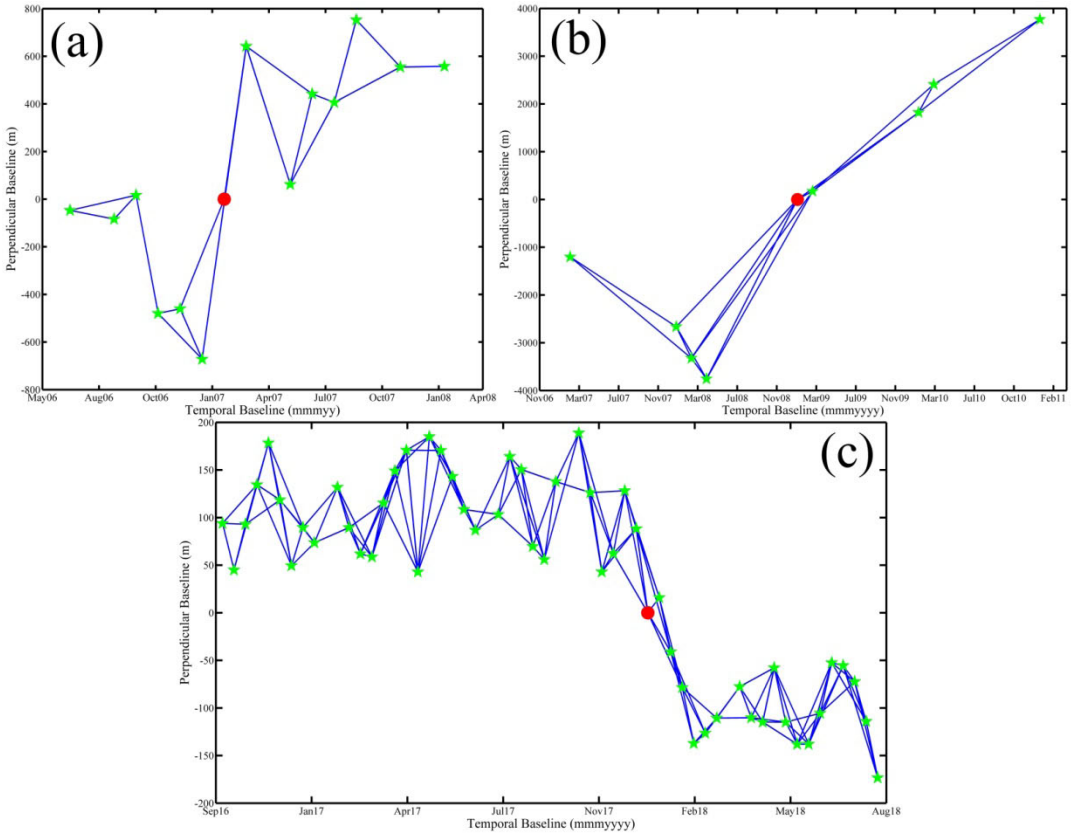

FIGURE 2. Spatiotemporal baseline map of interferometric pairs. The red dot denotes the master images, the green star denotes the slave images. (a) ENVISAT images; (b) ALOS-1 images; (c) Sentinel-1A images.

Therefore, a temporal coherence factor (γ_x) can be constructed:

$$\gamma_x = \frac{1}{\mathrm{N}} \left| \sum_{i=1}^{\mathrm{N}} \exp\left\{ \mathrm{j} \left(\varphi_{x,i} - \tilde{\varphi}_{x,i} - \Delta\emptyset^{u}_{\theta,x,i} \right) \right\} \right| \quad (4)$$

Since the value of δ is minimal, γ_x effectively reflects the noise contamination of the SDFPc. The greater the value of γ_x, the better the coherence of the SDFPc. Therefore, γ_x can be used to refine the SDFPc points. Phase unwrapping was then performed using a three-dimensional phase unwrapping algorithm [30], and the least-squares algorithm was used to convert the unwrapped phase ($\emptyset_{x,i}$) from multiple masters into a single master.

$$\emptyset_{x,i} = \emptyset_{D,x,i} + \emptyset_{A,x,i} + \Delta\emptyset_{Orb,x,i} + \Delta\emptyset^{c}_{\theta,x,i} + \emptyset_{N,x,i} + 2k_{x,i}\pi \quad (5)$$

where $\Delta\emptyset^{c}_{\theta,x,i}$ is the spatially correlated look error phase, while $2k_{x,i}\pi$ is the integer ambiguity. If the phase unwrapping was correct, the $2k_{x,i}\pi$ of all SDFP points in each interferometric pair will be the same, and the integer ambiguities can be removed using a reference point.

Finally, the deformation phase of each SDFP was obtained by spatial and temporal filtering.

IV. RESULTS

Fig. 3(a) shows the line-of-sight (LOS) deformation rates for the western Xuzhou coalfield obtained by ENVISAT images. Negative values indicate deformations away from the satellite (i.e., subsidence along the LOS) while positive values indicate deformations towards the satellite. In Fig. 3(a), it is shown that the ENVISAT images is severely affected by vegetation and temporal decorrelation, so the SDFP points were mostly located on buildings and exposed rocks, which were heterogeneously distributed across the study area, resulting in incomplete monitoring of deformation areas. The surface deformations were dominated by surface subsidence. Four significant areas of subsidence were detected in Zhangxiaolou mine, Pangzhuang mine, Jiahe mine, and in the southern part of Jiahe mine. The maximum subsidence rate located in the Zhangxiaolou mine was -164.6 mm/yr. The subsidence in the southern part of Jiahe mine was caused by coal mining in Daliu mine.

Fig. 3(b) shows the standard deviation (STD) of the LOS annual average deformation rates obtained by ENVISAT, which indicates that the STD of the zones with large-deformation rates in Zhangxiaolou mine, Pangzhuang mine, Jiahe mine, and the southern part of Jiahe mine are significant. The statistical analysis of the STD of all monitoring points (Fig. 6(a)) suggests that the standard deviations of 88.2% monitoring points are less than 15 mm/yr and 58.9% are less than 10 mm/yr. The average STD was 10.0 mm/yr.

The LOS annual average deformation rates obtained by ALOS-1 images is shown in Fig. 4(a). Since the high

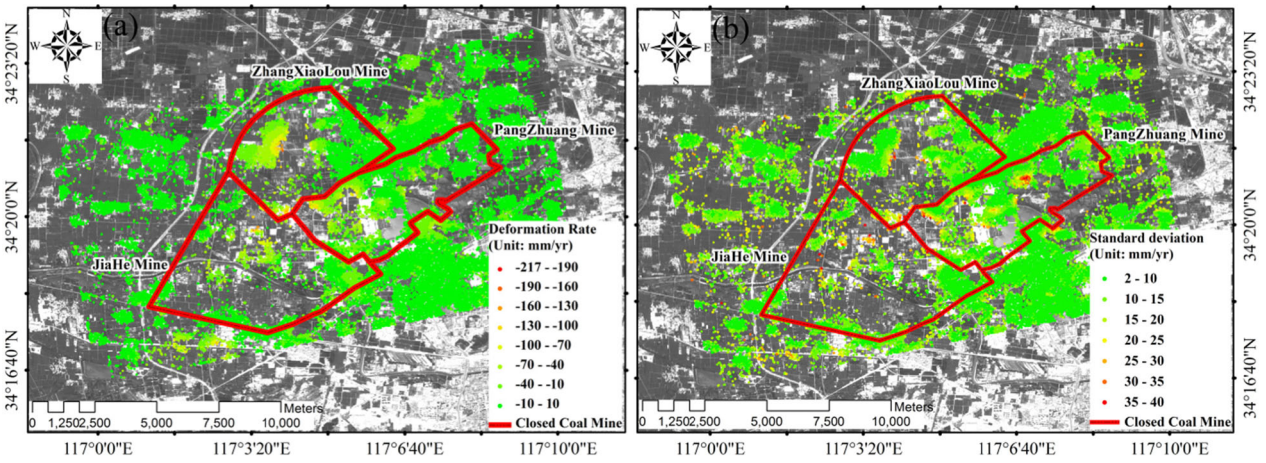

FIGURE 3. (a) The LOS annual average deformation rates obtained by ENVISAT. (b) The standard deviations of LOS annual average deformation rates.

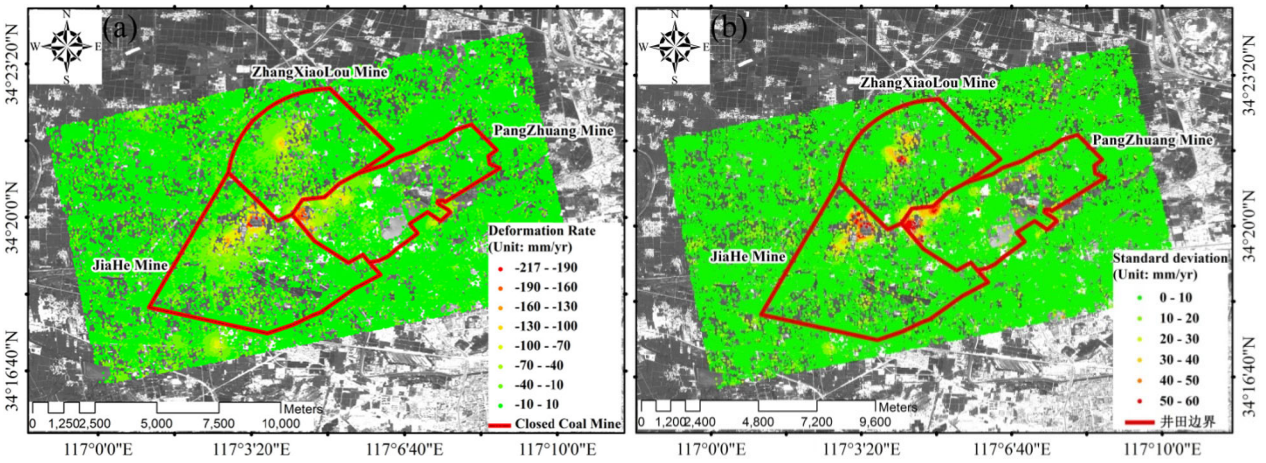

FIGURE 4. (a) The LOS annual average deformation rates obtained by ALOS-1. (b) The standard deviations of LOS annual average deformation rates.

resolution and long wavelength of ALOS-1 image, the effects from vegetation and temporal decorrelation were relatively minimal. As a result, ALOS-1 images with a time span of 4 years is superior to ENVISAT images with a time span of 1.5 years in terms of the number, density, and distribution of SDFP points. The results of ALOS-1 monitoring provided a much more complete surface deformation than ENVISAT. During the ALOS-1 monitoring period, four subsidence zones were identified, and the spatial locations of the deformations are consistent with those obtained by ENVISAT. Since the ENVISAT and ALOS-1 temporally coincide to some extent, the results of ALOS-1 monitoring may be treated as a continuation of ENVISAT. The maximum subsidence rate located in the Jiahe mine was −216.8 mm/yr. In addition, it was noted that the scope and magnitude of the subsidence in the southern part of Jiahe mine decreased during this period.

Fig. 4(b) shows that the STD of the LOS annual average deformation rates obtained by ALOS-1. Based on comparisons with Fig. 4(a), the locations with the large STDs always coincide with the areas that show the large deformations. The statistical analysis of the STD of all monitoring points (Fig. 6(b)) suggests that the standard deviations of 84.0% monitoring points are less than 15 mm/yr and 63.1% are less than 10 mm/yr. The average STD was 9.8 mm/yr.

The LOS annual average deformation rates obtained by Sentinel-1A images is shown in Fig. 5(a). After December 2015, all of the mines in western Xuzhou were closed. The surface deformation that occurred during Sentinel-1A monitoring period was relatively small and complex. Other than the subsidence that was detected in Zhangxiaolou mine, Pangzhuang mine, and Jiahe mine, uplift was also observed in the northeastern part in Pangzhuang mine, the central part in Jiahe mine, and in the northeastern part of Zhangxiaolou mine. However, the surface deformation that occurred between 2011 and 2015 could not be detected due to the absence of SAR data. The subsidence was observed in the northern part in Jiahe mine, with rates of up to

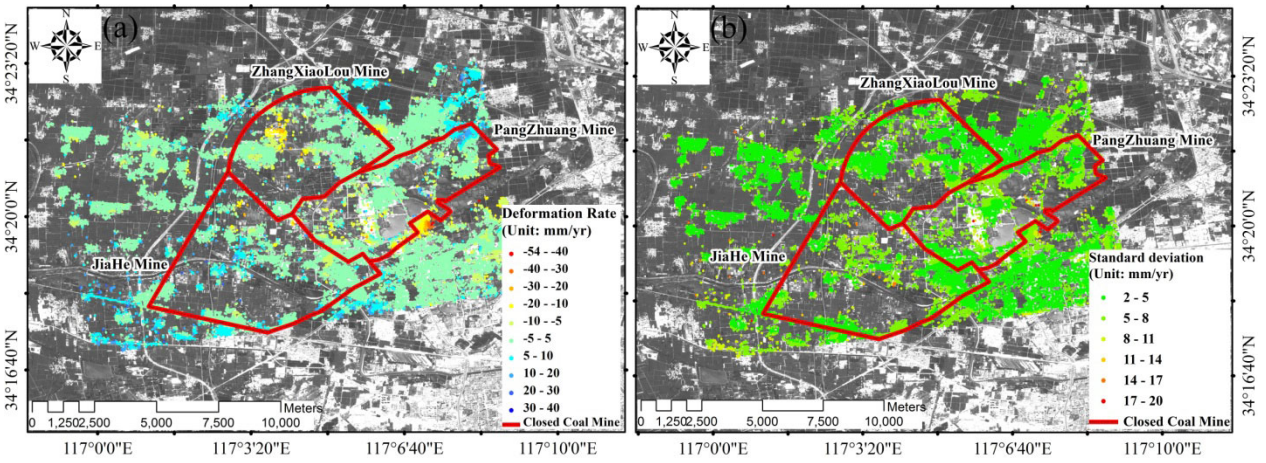

FIGURE 5. (a) The LOS annual average deformation rates obtained by Sentinel-1A. (b) The standard deviations of LOS annual average deformation rates.

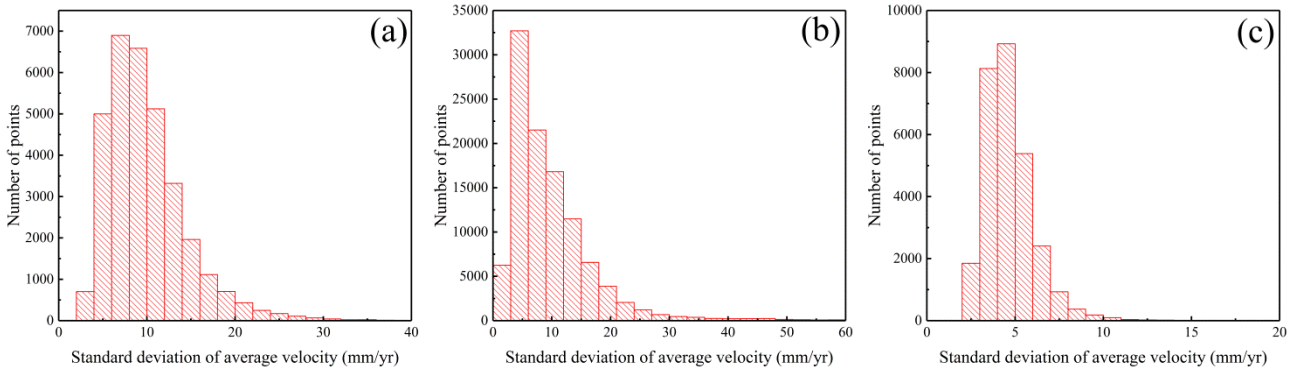

FIGURE 6. Statistical histogram of standard deviation of average deformation rate.

−29.4 mm/yr. Uplift occurred in the central parts in Jiahe mine, at rates of up to 24.6 mm/yr. The deformations in the Pangzhuang mine were dominated by subsidence in the southwest and uplift in the northeast, which reached a maximum of 26.5 mm/yr. A significant subsidence was observed at the southeastern margin of the Pangzhuang mine (rates up to −53.8 mm/yr) due to the mining activities in the Shitun mine.

Fig. 5(b) shows that the STD of the LOS annual average deformation rates obtained by Sentinel-1A. The statistical analysis of the STD of all monitoring points (Fig. 6(c)) suggests that the standard deviations of 99.2% monitoring points are less than 10 mm/yr and 66.5% are less than 5 mm/yr. The average STD was 4.7 mm/yr.

V. DISCUSSION

A. ACCURACY ASSESSMENT

Based on the STDs of the LOS annual average deformation rates (Figs. 3(b), 4(b)), it is shown that there is a significant spatial correlation between the STDs of the ENVISAT and ALOS-1 and the surface deformations. This is because mining activities were intense during the ENVISAT and ALOS-1 monitoring periods. This resulted in large surface deformations and strong non-linear deformations that gave rise to large residual deformations [3], [15]. The spatial correlation between the STD and surface deformation is not significant in the Sentinel-1A (Fig. 5(b)). This is because mining had already ceased during the Sentinel-1A monitoring period. The surface deformation was small, sustained over a long time, and had clear linear trend. Furthermore, interferometric pairs generated from the Sentinel-1A is redundant, the accuracy of deformation can be improved when time series InSAR analysis is carried out. Based on the statistical analysis of the STDs (Fig. 6), it was found that the results derived from ALOS-1 and ENVISAT have a similar level of accuracy, and the Sentinel-1A monitoring results are more accurate than those of both ALOS-1 and ENVISAT.

A total of 14 levelling points (9 in Jiahe mine, 5 in Zhangxiaolou mine) were used to validate the ALOS-1 monitoring results. The locations of the levelling points are shown in Fig. 7. Since the deformation obtained from the InSAR is the projection of three-dimensional deformation in the LOS, the accuracy analysis was conducted by converting the LOS

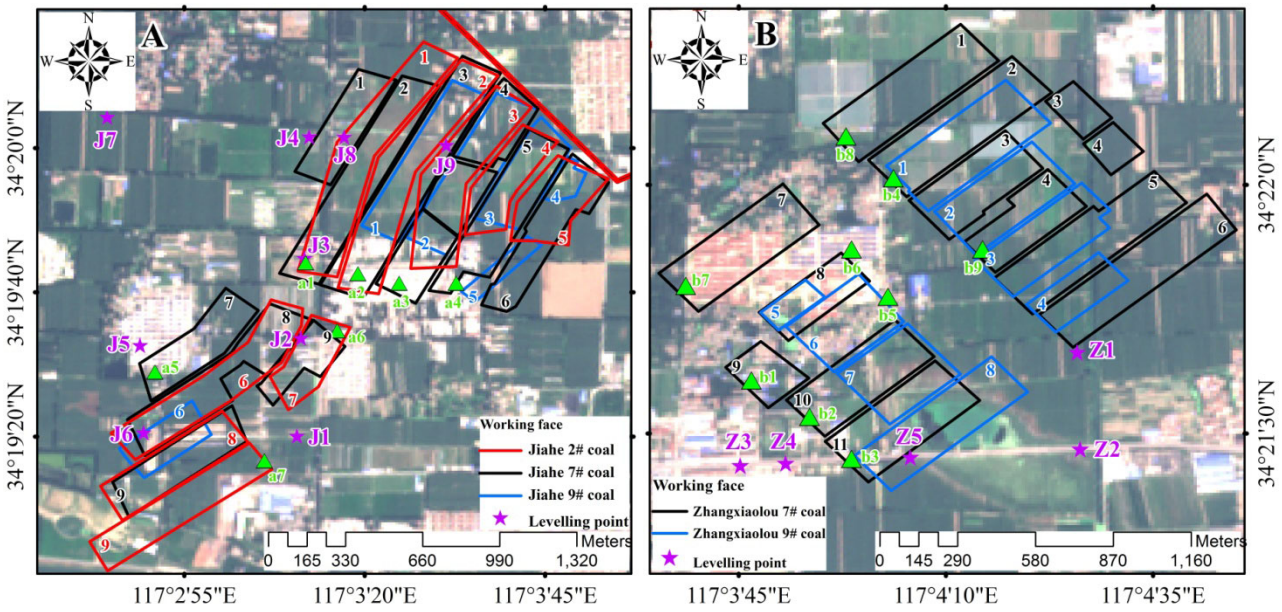

FIGURE 7. Overview of the selected area in Fig. 1. Green triangle represents the selected analysis points; red, black and blue numbers correspond to the working face of Table 3 and Table 4.

TABLE 2. Accuracy evaluation of InSAR results.

	J1	J2	J3	J4	J5	J6	J7	J8	J9	Z1	Z3	Z4
MaxD (mm)	47.9	30.2	37.9	51.2	45.6	89.8	35.2	37.9	140.0	35.5	51.5	43.3
MinD (mm)	15.2	0.3	15.8	1.6	11.3	18.4	1.7	2.9	33.4	12.9	0.04	1.9
RMSE (mm)	28.6	15.8	26.3	29.5	27.1	52.9	19.3	25.5	83.1	20.8	27.9	24.6
STD (mm)	30.9	16.7	28.2	23.7	30.1	57.9	17.9	20.9	73.1	15.3	17.0	15.3

deformation into vertical deformation without considering horizontal movement.

As it is difficult to ensure that coherent points are located at the levelling points, the deformation at each levelling point was compared to the average deformation of the coherent points within 50 m of the levelling point. The comparison results are shown in Fig.8. The subsidence trend and magnitude of time-series deformation derived from the ALOS-1 at the J1 – J9, Z1, Z3, and Z4 are consistent with levelling data. Although the subsidence trend at Z2 and Z5 is consistent with levelling data, they differ significantly in order of magnitude. The deformation at the Z5 reached a maximum of 1.22 m, but the deformation acquired by the ALOS-1 was only half this value. This can be attributed to the relative scarcity of ALOS-1 image, although the wavelength of ALOS-1 image is longer, the time span is too long. Consequently, the deformation that occurred between the two images exceeded the maximum detectable deformation gradient, which led to errors in the phase unwrapping and the underestimation for surface deformation.

To quantitatively assess the accuracy of the monitoring results, the InSAR time-series deformation and levelling data of Jiahe mine and Zhangxiaolou mine were linearly interpolated to coinciding points in time. Since the actual deformation at Z2 and Z5 at Zhangxiaolou mine exceed the maximum detectable deformation gradient by InSAR, accuracy assessments were not performed at these points. As the J5, J6 points at Jiahe mine exhibit pronounced non-linear deformation and the temporal frequency of the InSAR results was relatively low, the levelling data at these points were linearly interpolated to the InSAR time series. The accuracy of the InSAR results was evaluated in terms of maximum deviation (MaxD), minimum deviation (MinD), root mean square error (RMSE), and STD. The results of the evaluation are shown in Table 2.

From Table 2, it is shown that the accuracy of all points other than J6 and J9 was less than 30 mm. The average RMSE and STD of these points are 31.8 mm and 28.9 mm, respectively. The factors affecting accuracy may be attributed to the following: (a) Only a few ALOS-1 images were acquired during the monitoring period. Although the L-band has a large detectable deformation gradient and is relatively insensitive to vegetation and temporal decorrelation, the lengthy time intervals between ALOS-1 images led to a large deformation

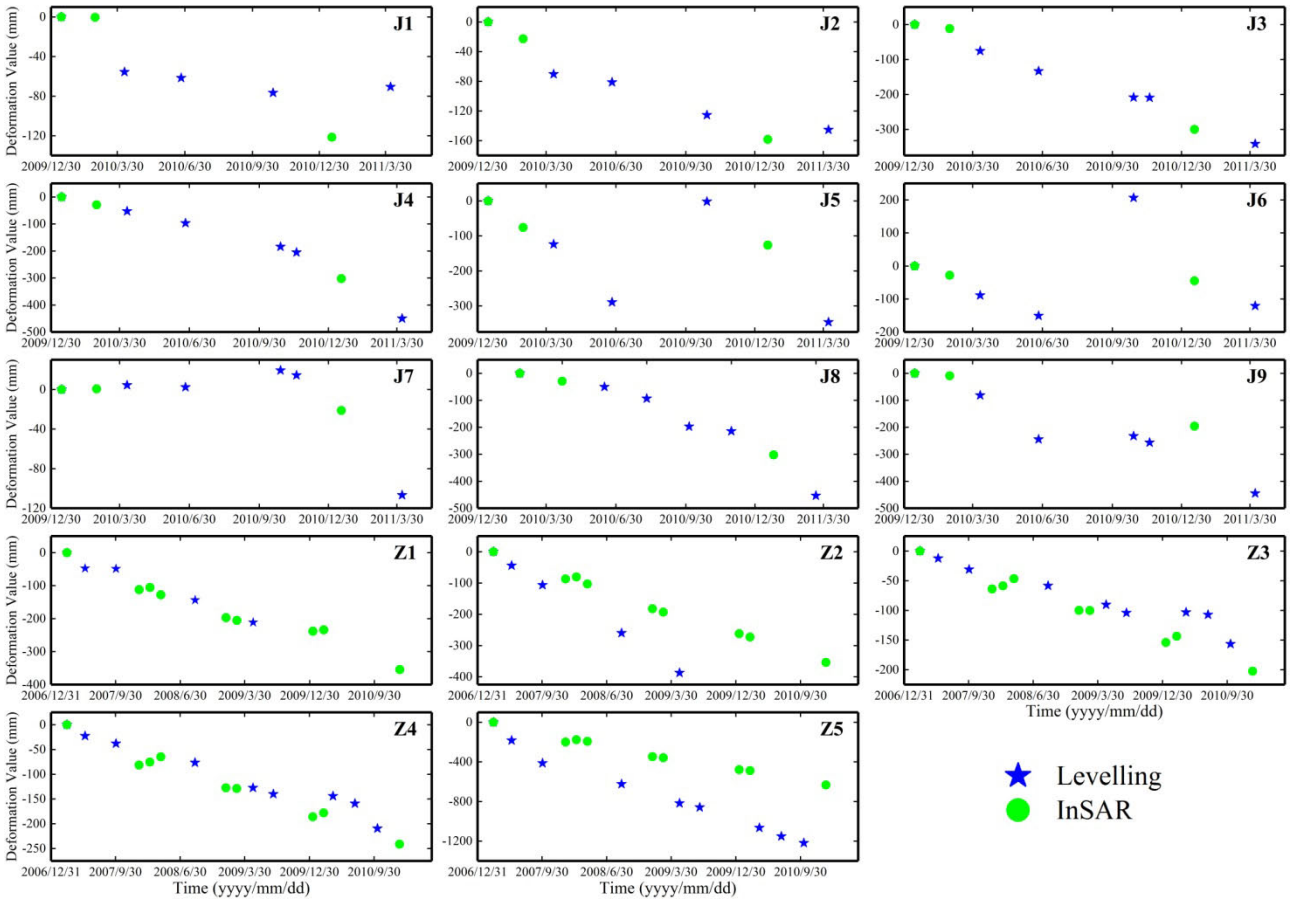

FIGURE 8. Comparison of levelling data and InSAR results.

gradient. (b) Due to large surface deformation can occur in mine areas in a relatively short time, which leads to significant non-linear deformations. The use of linear interpolation to compare the InSAR results with the levelling data will therefore inevitably lead to a lower level of accuracy. Furthermore, the InSAR deformation at each levelling point was obtained by averaging the deformations at coherent points within 50 m of the levelling point, which affects the comparison. (c) Due to deformation in mining areas tend to be accompanied by large horizontal movement [7]. For example, a maximum subsidence of 1.22 m was measured at the Z5 levelling point, based on the geological mining conditions of Xuzhou's mining areas the maximum horizontal movement ($U_{\max}$) is at least 378 mm ($U_{\max} = bW_{\max}$, where $W_{\max}$ is the maximum subsidence and b is the horizontal movement coefficient of 0.31). Therefore, the neglection of horizontal movement will affect the accuracy evaluation. In summary, it has been shown that the accuracy of ALOS-1 monitoring results can reach the centimetre level, which is sufficient for detecting surface deformation induced by mining.

The statistical analysis of the STDs (Fig. 6) shows that the accuracy of ALOS-1 and ENVISAT monitoring results are similar, and that the Sentinel-1A monitoring results are more accurate. Hence, it can be concluded that the accuracy of the deformations derived from the three SAR datasets reached or better than the centimetre level.

B. DEFORMATION ANALYSIS OF WESTERN XUZHOU COALFIELD

1) DEFORMATION ANALYSIS OF JIAHE MINE

In Figs. 3(a), 4(a), since most of the underground mining was occurring in the northwestern part in Jiahe mine (as shown in Figs. 1, 7, and Table 3). Therefore, surface subsidence detected by ENVISAT and ALOS-1 was caused by underground mining. After Jiahe mine closure, the surface deformation became more complex. The residual subsidence that occurred in the northern part in Jiahe mine (Fig. 5(a)) could be attributed to the large mining depth of the working face (the maximum mining depth was 1190 m), since surface subsidence persists for longer durations on deep working faces [31]. Alternatively, the rise in groundwater levels may have re-compacted the broken rocks in goaf which resulted in secondary subsidence [32]. The surface uplift that occurred in central Jiahe mine may have been caused by the rise in groundwater levels after the mine closure, which would have increased the hydraulic pressure and resulted in an upwards force on the overburden. The increase in pore water pressure

TABLE 3. Working face information of zone A in Jiahe mine.

Working face	Mining time	Thickness (m)	Depth (m)	Working face	Mining time	Thickness (m)	Depth (m)
2# 1	2010.7-2011.11	2.3	1018	7# 4	2005.11-2007.3	2.1	970
2# 2	2008.3-2009.9	2.0	947	7# 5	2007.10-2008.9	2.1	921
2# 3	2005.5-2006.6	2.0	857	7# 6	2009.11-2010.10	2.2	820
2# 4	2003.11-2004.9	2.0	792	7# 7	2013.9-2014.3	2.4	1150
2# 5	2006.3-2007.3	2.1	716	7# 8	2007.3-2008.3	2.3	1140
2# 6	2011.11-2013.1	1.8	1020	7# 9	2009.3-2010.6	2.3	1050
2# 7	2009.10-2010.3	1.8	965	9# 1	2014.12-2015.9	2.1	1090
2# 8	2006.9-2007.8	2.2	960	9# 2	2008.9-2009.6	2.8	1016
2# 9	2006.6-2007.8	2.2	900	9# 3	2010.11-2011.4	2.2	917
7# 1	2015.5-2015.9	2.3	1190	9# 4	2010.11-2011.4	2.2	854
7# 2	2014.3-2014.12	2.2	1140	9# 5	2012.5-2012.9	3.4	904
7# 3	2012.8-2013.8	2.5	1075	9# 6	2013.2-2013.10	1.1	1154

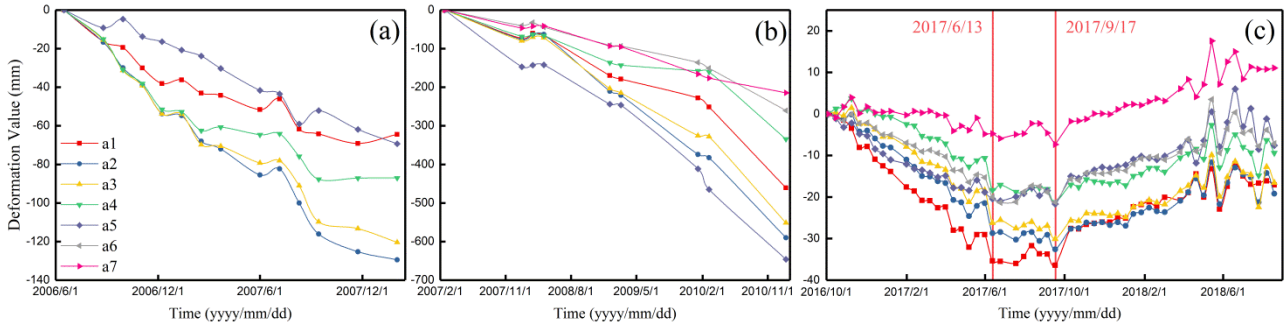

FIGURE 9. Seven points time-series deformations in Jiahe mine.

between the broken rocks in goaf could also have reduced the effective stresses of the overburden, thus resulting in the elastic deformation recovery and surface uplift [33], [34].

To analyse the law of surface deformation in Jiahe mine, seven points were selected in zone A (as shown in Fig. 7(A)) according to working face information.

Since the results of ENVISAT does not contain any coherent points around a6 and a7, LOS time-series deformations could only be obtained at the five remaining points (a1 – a5), the results were shown in Fig. 9 (a). Prior to the closure of Jiahe mine, the results of ENVISAT show that underground mining led to subsidence at all five of these points. The maximum cumulative subsidence of −129.5 mm occurred at a2, followed by −120.4 mm at a3. Based on the information in Table 3 and Fig. 7(A), the only active working faces were those under a3, a4, and a7 during the ENVISAT monitoring period. Due to the tilt of the coal seam (about 20°), the subsidence at a2 was therefore greater than that at a3 because a2 is downhill (northwest) in the subsidence basin. Although the working face below a4 was being excavated, the subsidence at a4 was less than that at a2 and a3 because the a4 point is located uphill. The subsidence at a1 and a5 was relatively small since these points are located at a considerable distance from the active working faces.

As shown in Fig. 9 (b), during the ALOS-1 monitoring period, all seven points exhibited LOS time-series subsidence. The maximum cumulative subsidence of −646.6 mm occurred at a5. Based on the information in Table 3 and Fig. 7(A), other than a5, working faces were being excavated under all of the other points. However, the subsidence at a5 was still significant. This is because a5 was being affected by the excavation of nearby working faces (7# 8), and the tilt of the coal seam caused the subsidence basin to shift downhill (northwest). Based on the relative positions of the selected points and working faces, it was found that a5 was located at the centre of the subsidence basin, and the other points were located around the margin of the subsidence basin. The subsidence of a4, a6, and a7 was relatively minimal since these points were located uphill of the working faces.

After the closure of Jiahe mine, residual subsidence occurred at all points other than a7 prior to 13/6/2017

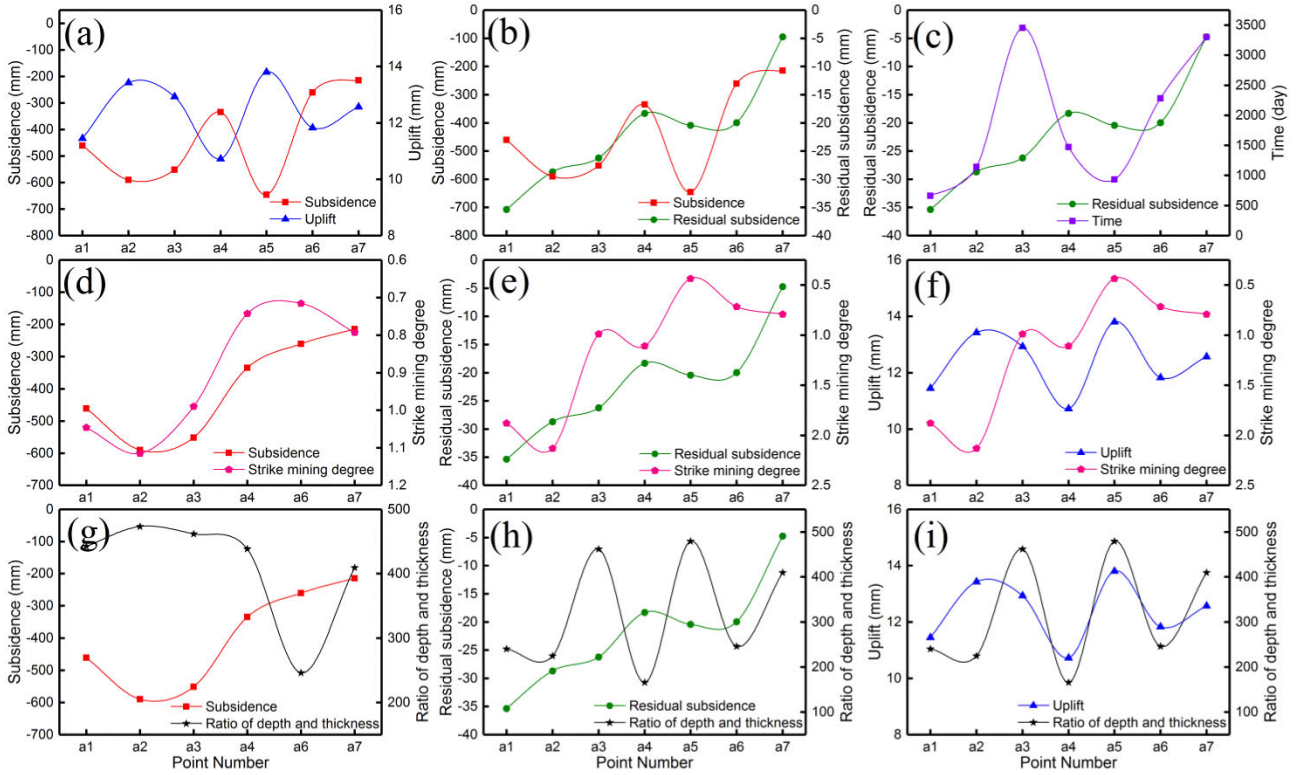

FIGURE 10. Analysis of deformation law of Jiahe mine.

(As shown in Fig. 9 (c)). The maximum cumulative subsidence of −35.4 mm occurred at a1, followed by −28.7 mm at a2. After 17/9/2017 surface uplift occurred at all seven points. The maximum cumulative uplift of 13.8 mm occurred at a5. Based on the time-series deformation at these seven points, there was a stability period between the end of the residual subsidence and the beginning of the uplift (13/6/2017– 17/9/2017). This is because the factors that lead to surface subsidence (e.g., residual subsidence over the goaf, secondary subsidence in broken rock due to groundwater) and surface uplift (e.g., increases in pore pressure due to rising groundwater levels) effectively nullified each other. Alternatively, the broken rocks in goaf may have been recompacted by groundwater or other factors, which redistributed the stress on the overburden and led to a state of relative stability. During the Sentinel-1A monitoring period, the surface deformation at Jiahe mine was characterised by a residual subsidence and a subsequent stability period, followed by surface uplifting.

The relationship between the surface deformation before and after mine closure was analysed at these seven points, the results are shown in Fig. 10. The analysis of the relationship between the deformation during mining and other factors was based only on the results of ALOS-1, since the results of ENVISAT does not include any deformation at a6 and a7. Fig. 10(a) indicates that the surface subsidence during mining are positively correlated with the surface uplift that occurred after the mine closure, with a correlation coefficient of 0.65. The locations where large surface subsidence during mining also exhibited significant uplift after mine closure. This is because of the downward displacement of the rock strata was also significant in large-subsidence locations, and groundwater loss was serious. Groundwater levels rapidly rebound after the mine was closed, which increased the pore pressure and led to a large elastic deformation recovery [6], [35], [36]. In Fig. 10(b), it is shown that the subsidence during mining is positively correlated with the residual subsidence that occurred after the mine was closed, with a correlation coefficient of 0.62. The greater the surface subsidence during mining, the greater the residual subsidence that occurs after mine closure. This may be because bed-separated fissures are highly developed in the overburden in locations that exhibit large surface subsidence, which are readily ''activated'' by groundwater.

To analyse the law of surface deformations that occurred before and after mine closure, the deformations at these seven points were analysed, based on the working faces information. The depth and thickness at the points that were repetitive mining correspond to the average depth and total thickness of the working faces at these points, respectively. Based on Fig. 10(c), surface residual subsidence is approximately negatively correlated with the time that elapsed after working face mining had ceased, with a correlation coefficient of −0.56. After the closure of a mine, the surface residual deformation decreased over time, which is consistent with the law of mining subsidence [37]. During the ALOS-1 monitoring

TABLE 4. Working face information of zone B in Zhangxiaolou mine.

Working face	Mining time	Thickness (m)	Depth (m)	Working face	Mining time	Thickness (m)	Depth (m)
7# 1	2014.4-2014.12	2.9	1168	7# 11	2006.11-2007.6	1.86	1130
7# 2	2012.4-2012.12	2	1138	9# 1	2013.11-2014.12	2.2	1154
7# 3	2010.10-2011.10	1.8	1120	9# 2	2011.11-2012.6	2	1136
7# 4	2009.11-2010.2	1.8	1107	9# 3	2010.7-2011.1	1.8	1133
7# 5	2007.12-2008.7	1.8	1140	9# 4	2009.1-2009.6	2	1138
7# 6	2006.3-2006.11	1.7	1006	9# 5	2015.7-2015.9	1.8	1106
7# 7	2013.5-2014.2	1.75	1128	9# 6	2014.12-2015.6	1.8	1116
7# 8	2011.10-2012.4	1.9	1101	9# 7	2012.12-2013.5	2.4	1131
7# 9	2010.4-2010.8	1.9	1072	9# 8	2011.5-2012.2	2.4	1131
7# 10	2008.4-2008.10	1.8	1140				

period, the working face below a5 had yet to be excavated. Therefore, the relationship between surface deformation during mining and working face was only analysed at the other points. From Fig. 10(d) it is apparent that surface subsidence during mining is positively correlated with strike mining degree; the greater this degree the larger the subsidence. The correlation coefficient is 0.90. This is because the deep mining, the surface subsidence is often insufficient, and the mining degree plays a significant role in controlling surface subsidence. The greater the mining degree, the more fully the surface subsidence is, until maximum subsidence is reached [38]. In Fig. 10 (e), it is demonstrated that the post-mine closure residual subsidence decrease as the strike mining degree is diminished, with a correlation coefficient of 0.70. This is because the bed-separated fissures of the overburden intensifies with increases in the strike mining degree. These fissures are easily ''activated'' by rising groundwater levels after mine closure, which then leads to significant residual deformations. In Fig. 10(f), it may be observed that the surface uplift that occur after mine closure is only weakly related to the strike mining degree. In Figs. 10(g) and (h), it is shown that the depth-to-thickness ratio of working face is not significantly correlated to the surface subsidence that occurs before and after mine closure. By comparing with Figs. 10(d) and (e), it is suggested that the effect that the thickness of the working face has on subsidence are weaker than those from the dimensions of the working face in deep mining. Fig. 10(i) shows that the surface uplift that occur after mine closure is positively correlated with the depth-to-thickness ratio of working face with a correlation coefficient of 0.70. This is because groundwater will initially begin to accumulate in the deeper working faces after a mine is closed, resulting in high water pressure at the deeper working faces and a correspondingly large surface uplift.

2) DEFORMATION ANALYSIS OF ZHANGXIAOLOU MINE

Based on Figs. 3(a), 4(a), it shown that the results of ENVISAT and ALOS-1 both indicate a subsidence in the central part in Zhangxiaolou mine (zone B in Fig. 1). This is because underground mining was mainly conducted in this area (as shown in Fig. 7 (B) and Table 4). Based on the results of Sentinel-1A (Fig. 5(a)), the surface still show a significant subsidence in this area after the mine closure. This can be attributed to the large mining depth in Zhangxiaolou mine, at an average depth of 1122 m and a maximum depth of 1168 m (as shown in Table 4). The mining depth led to surface subsidence that persisted for extended periods and the surface subsidence is insufficient, which resulted in large residual subsidence [31]. However, it is also possible that groundwater may have filled the deep areas of the mine and caused the broken rocks in the goaf to continue compaction [32], thus leading to surface subsidence.

To analyse the law of surface deformation of Zhangxiaolou mine, nine points were selected in zone B (as shown in Fig. 7(B)) according to the information of working face.

The time-series LOS deformations of the nine points are shown in Fig. 11. Since the ENVISAT results does not have any coherent points near b9, the ENVISAT results only include the subsidence of the eight remaining points, the results were shown in Fig. 11 (a). The maximum subsidence occurred at b3 (−118.4 mm). Based on the locations of the points in zone B (Fig. 7) and the working faces information (Table 4), only the working face under b3 was still active. Therefore, the deformation at b3 point was the largest. Based on the spatial relationship between other points and the working face under b3, it was found that the deformation at each point was inversely related to its distance from the working face under b3; the greater this distance, the smaller the deformation.

Fig. 11(b) shows that time-series subsidence occurred at all nine points during the ALOS-1 monitoring period. The maximum subsidence of −397.2 mm occurred at b3, the minimum subsidence of −56.6 mm occurred at b8. According to the information in Fig. 7(B) and Table 4, it was found that the working faces under points b1, b2, and b9, and

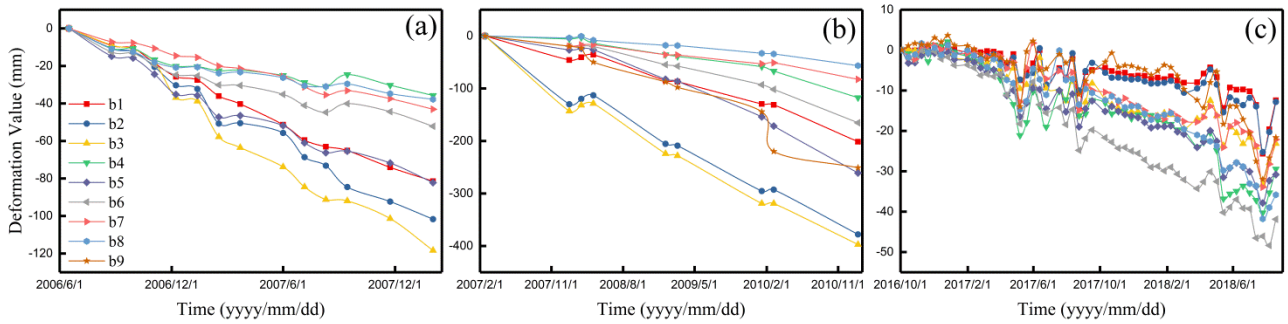

FIGURE 11. Nine points time-series deformations in Zhangxiaolou mine.

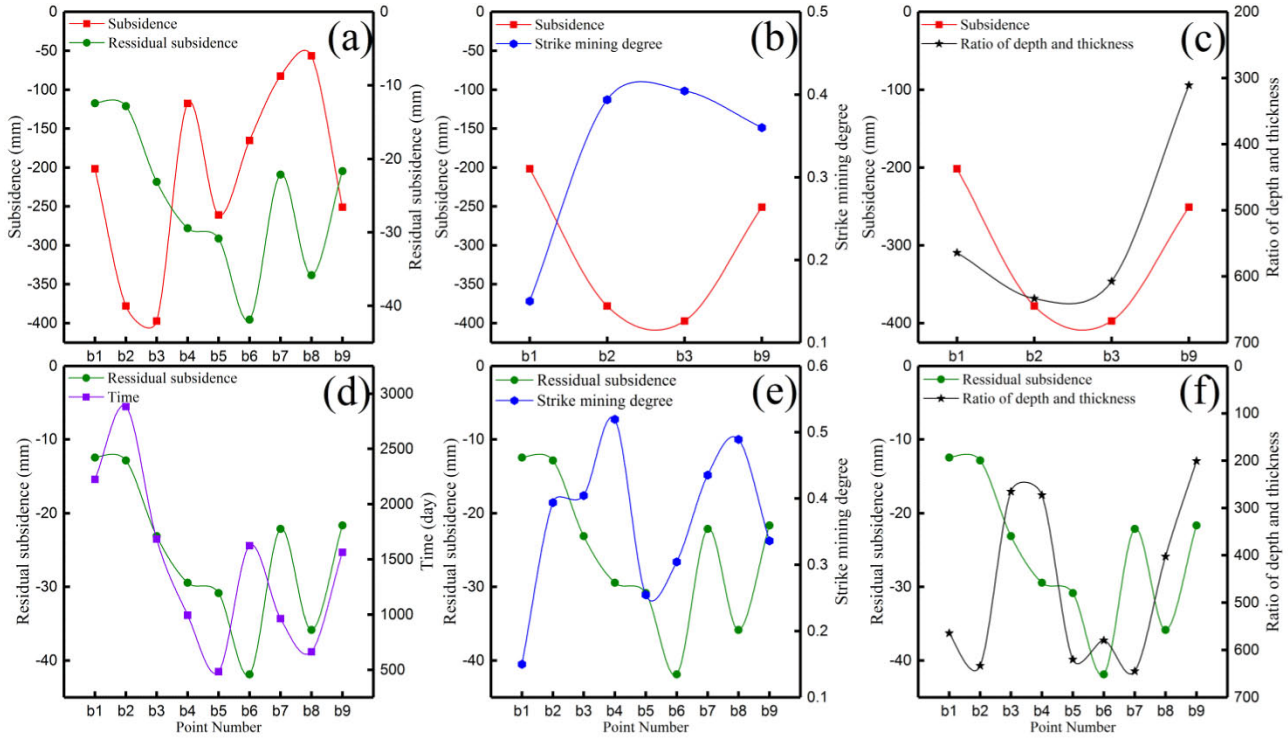

FIGURE 12. Analysis of deformation law of Zhangxiaolou mine.

a part of the working face under b3, were being mining. The mining degree under b1 was minimal as it had the smallest dimensions between working faces. Consequently, the surface deformation caused by the excavation of the working face under b1 was also relatively small. The deformation at b1 was mainly caused by the excavation of adjacent working faces. Therefore, the surface subsidence at b1 was small compare to that of b2, b3, and b9 during mining. Since the working faces under b4, b5, b6, b7, and b8 had yet to be excavated, the deformations at these points were caused by the excavation of nearby working faces. The magnitude of the subsidence depended on the distance from the excavated working faces.

After the closure of Zhangxiaolou mine, except that b9 point was stable up to 4/3/2018, and then began to subside rapidly, the eight other points exhibited time-series subsidence (see Fig. 11(c)). The maximum subsidence of −41.9 mm occurred at b6, the minimum subsidence of −12.4 mm occurred at b1. The deformations detected at these nine points exhibited large fluctuations during the summer. This may have been caused by the precipitation that fell during the June – August period, which accounts for 60% of the annual precipitation in the study area [39].

The relationship between the surface deformation before and after mine closure was analysed at the nine points. The results are shown in Fig. 12. The analysis of the relationship between the deformation during mining and other factors was based only on the results of ALOS-1, since the results of ENVISAT does not include any deformation at b9. In Fig. 12(a), it is shown that the deformation during mining

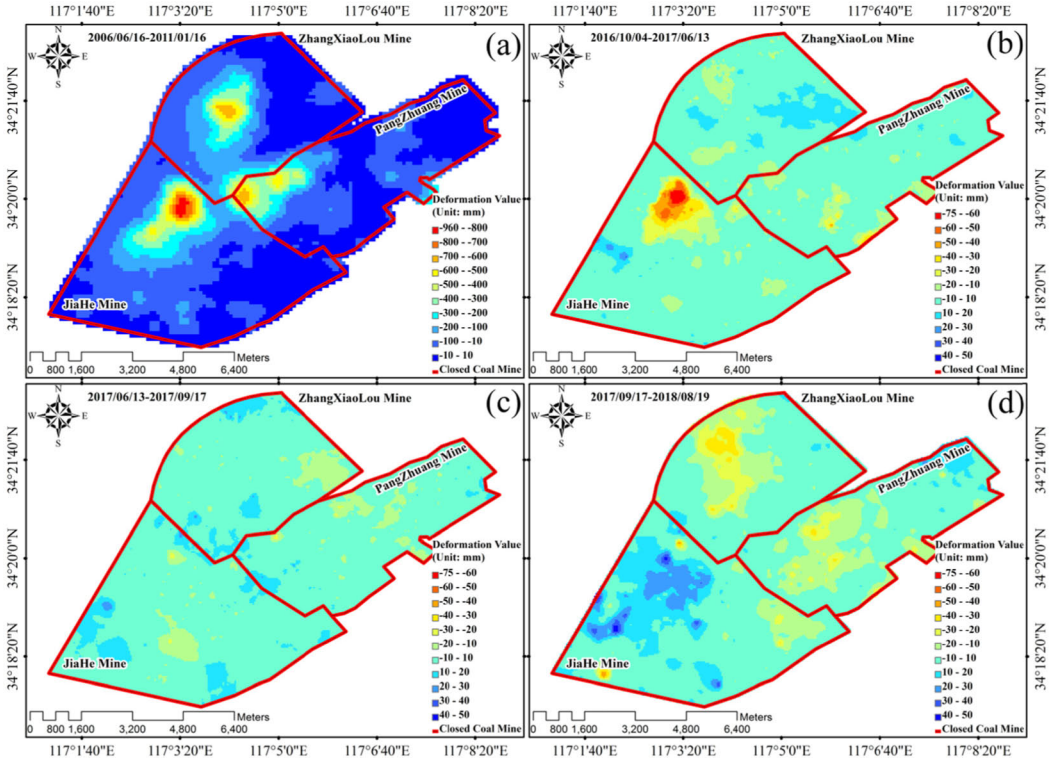

FIGURE 13. Deformation development process in western Xuzhou coalfield.

is weakly correlated with the deformation that occurred after the mine closure. This is because most of the working faces in zone B were not being excavated during the ALOS-1 monitoring period (as shown in Table 4), which resulted in a lack of correlation between the surface deformation that occurred before and after mine closure.

The only working faces that were being excavated during the ALOS-1 monitoring period are located under b1, b2, b3, and b9. The relationship between the surface deformation and working face during mining was therefore only analysed at these points. In Fig. 12(b), it is apparent that surface deformation is positively correlated to the strike mining degree, with a correlation coefficient of 0.83. The relationship between the surface deformation during mining and the thickness-to-depth ratio of the working face is shown in Fig. 12(c), with a correlation coefficient of 0.54. This observation appears to contradict the expected law of mining subsidence. Because the deformations at b1 were mainly caused by the excavation of nearby working faces. Hence, the actual response of surface deformation to the thickness-to-depth ratio of a working face was not revealed by the analysis of b1, b2, b3, and b9. Based on Fig. 12(d), surface residual subsidence is approximately negatively correlated with the time that elapsed after working face mining had ceased, with a correlation coefficient of -0.65. In Figs. 12(e) and (f), it is shown that the surface residual subsidence is not significantly correlated to the strike mining degree and depth-to-thickness ratio of the working face.

3) ANALYSIS OF OVERALL DEFORMATION

In order to better clarify the deformation law of the western Xuzhou coalfield, inverse distance weighting interpolation was used to obtain the overall vertical deformation of the study area before and after mine closure. Since the ENVISAT and ALOS-1 images coincide with each other temporally, reference time of the ALOS-1 results was normalized onto that of the ENVISAT (16/6/2006). From the analysis of section 5.2.1, it is shown that there are three stages in the Sentinel-1A monitoring period in Jiahe mine. Therefore, the monitoring results of Sentinel-1A are divided into three time periods, taking 13/06/2017 and 17/09/2017 as the dividing points. The result is shown in Fig. 13. Fig. 13 (a) is the result of surface vertical cumulative deformation in the western Xuzhou coalfield from 16/06/2006 to 16/01/2011. The large-area subsidence in the western Xuzhou coalfield caused by mining, the maximum subsidence can reach $-$ 957 mm, which is smaller than the actual subsidence. Taking 10 mm subsidence as boundary, the overall subsidence area is about 43.93 km^2, accounting for 72.8% of the western Xuzhou coalfield.

One year after Jiahe mine and Zhangxiaolou mine were closed, the scope and magnitude of the subsidence in Zhangxiaolou mine were significantly smaller than those of Jiahe mine (Fig. 13(b)). According the geological report of Zhangxiaolou and Jiahe mines [40], [41], it was shown that the normal water inflow at Jiahe mine is 2 – 3 times that of Zhangxiaolou mine and the mining depth of Jiahe mine (average mining depth 982m) were generally shallower than

those of Zhangxiaolou mine (average mining depth 1122m). Therefore, groundwater levels rose rapidly after the closure of Jiahe mine, leading to rapid recompaction of its broken rocks, and the surface response time is shorter than Zhangxiaolou Mine [42], which resulted in significant surface subsidence in Jiahe mine. Because of the large mining depth at Zhangxiaolou mine the residual deformation persist for a long period of time [31], and the response time of surface deformation will be also long due to groundwater rises slowly. Therefore, the surface deformation that was observed in Zhangxiaolou mine during this period may correspond to the residual subsidence of goaf.

Fig. 13(c) shows that the surface of Jiahe mine was relatively stable during this period, which is consistent with the time-series deformation analysis shown in Fig. 9(c). Approximately two years after the Jiahe and Zhangxiaolou mines closure, uplift began to occur in Jiahe mine, and the severity of the subsidence in Zhangxiaolou mine increased significantly (Fig. 13(d)). In Jiahe mine, after the initial subsidence had stabilised, further increases in groundwater levels then led to surface uplifts. In Zhangxiaolou mine, which has much smaller water inflows and deeper mining depths [41], the response of the surface to rising groundwater levels was much slower, therefore, rapid subsidence occurred in Zhangxiaolou mine two years after its closure.

In Figs. 13(b), (c), and (d), it is shown that the surface deformation law of Pangzhuang mine are similar to those of Zhangxiaolou mine, the surface subsidence changed from slow subsidence to accelerated subsidence. The reason may be that the closure of Pangzhuang mine (2012 year) occurred at an earlier time than Zhangxiaolou mine and Jiahe mine, and Pangzhuang mine also had shallower mining depths than the two other mines. Since Zhangxiaolou and Jiahe mines were still active when Pangzhuang mine was closed, the rebound in groundwater levels at Pangzhuang mine was small, and the Sentinel-1A results shown that the surface deformation of Pangzhuang mine was mainly residual subsidence over goaf during the initial stage (Fig. 13(b)). When Zhangxiaolou and Jiahe mines were closed, the rebound in groundwater levels at Pangzhuang mine became more pronounced, which resulted in the recompaction of broken rocks by rising groundwater levels. Therefore, the rate and scope of surface subsidence in Pangzhuang mine increased significantly (Fig. 13(d)).

According to the law of surface deformation after Jiahe, Zhangxiaolou and Pangzhuang mines closure, we can be inferred that, after western Xuzhou coalfield closure, the surface deformation of may have been caused by residual subsidence over goaf, which was subsequently exacerbated by groundwater-related factors; a period of relative stability then took place which was followed by surface uplifts induced by the continuing rise of the groundwater levels.

VI. CONCLUSION

In this study, the surface deformation that occurred before and after mine closure in the western Xuzhou coalfield was obtained from 77 SAR images, based on the StaMSBAS technique. The surface deformation during mining was dominated by time-series subsidence. After the closure of the mine, the surface deformation became more complex due to the combined effects of goaf and groundwater, which resulted in surface uplift in some areas. By comparing AlOS-1 monitoring result to levelling data, it was shown that the average RMSE and STD were 31.8 mm and 28.9 mm, respectively. Combined with the STDs of the InSAR monitoring results analysis, it was concluded that the accuracy of the results acquired by ALOS-1, ENVISAT, and Sentinel-1A datasets either reached or exceeded the centimetre level.

The law of surface deformation that occurred before and after mine closure was analysed. During mining, the surface deformation of the western Xuzhou coalfield was dominated by time-series subsidence. After the mine closure, the surface deformation of Jiahe mine experienced the process of subsidence, relative stability and then uplift, and the surface deformations of Pangzhuang and Zhangxiaolou mines changed from slow subsidence to accelerated subsidence. Where the large subsidence during mining occurred at Jiahe mine, the surface uplift and residual subsidence that occurred after mine closure was also significant, correlation coefficients were 0.65 and 0.62, respectively. After mine closure, residual subsidence at Jiahe mine was positively correlated with the strike mining degree, and the surface uplift in this area was positively correlated with the depth-to-thickness ratio of working face, correlation coefficients were both 0.70.

After the closure of mines in western Xuzhou coalfield, the surface deformation may have been caused by residual subsidence over goaf, which was subsequently exacerbated by groundwater-related factors; a period of relative stability then took place, followed by surface uplifts, which was induced by the continuing rise of the groundwater levels.

REFERENCES

[1] *13th Five-Year Plan for Coal Industry Development*, Nat. Develop. Reform Commission, Beijing, China, 2016.

[2] L. Ping, "The activation, transformation, and updates of the abandoned mining area: Take the Quantai, Xuzhou mining area's concept design of landscape for example," in *Proc. 2nd Int. Conf. Consum. Electron., Commun. Netw.*, Apr. 2012, pp. 3547–3550.

[3] Z. Meinan, K. Deng, H. Fan, and S. Du, "Monitoring and analysis of surface deformation in mining area based on InSAR and GRACE," *Remote Sens.*, vol. 10, no. 9, p. 1392, 2018.

[4] M. C. Cuenca, A. J. Hooper, and R. F. Hanssen, "Surface deformation induced by water influx in the abandoned coal mines in Limburg, The Netherlands observed by satellite radar interferometry," *J. Appl. Geophys.*, vol. 88, pp. 1–11, Jan. 2013.

[5] H. Fan, L. Lu, and Y. Yao, "Method combining probability integration model and a small baseline subset for time series monitoring of mining subsidence," *Remote Sens.*, vol. 10, no. 9, p. 1444, 2018.

[6] H. Fan, Q. Xu, Z. Hu, and S. Du, "Using temporarily coherent point interferometric synthetic aperture radar for land subsidence monitoring in a mining region of Western China," *Proc. SPIE*, vol. 11, no. 2, 2017, Art. no. 026003.

[7] M. Zheng, K. Deng, H. Fan, and J. Huang, "Monitoring and analysis of mining 3D deformation by multi-platform SAR images with the probability integral method," *Frontiers Earth Sci.*, vol. 13, no. 1, pp. 169–179, 2019.

[8] Z. W. Li, Z. F. Yang, J. J. Zhu, J. Hu, Y. J. Wang, P. X. Li, and G. L. Chen, "Retrieving three-dimensional displacement fields of mining areas from a single InSAR pair," *J. Geodesy*, vol. 89, no. 1, pp. 17–32, 2015.

[9] R. L. Bamler and P. Hartl, "Synthetic aperture radar interferometry," *Inverse Problems*, vol. 14, no. 4, p. R1, 1998.
[10] Y. Fialko, M. Simons, and D. Agnew, "The complete (3-D) surface displacement field in the epicentral area of the 1999 M_W7.1 hector mine earthquake, California, from space geodetic observations," *Geophys. Res. Lett.*, vol. 28, no. 16, pp. 3063–3066, 2001.
[11] Z. Lu, E. Fielding, M. R. Patrick, and C. M. Trautwein, "Estimating lava volume by precision combination of multiple baseline spaceborne and airborne interferometric synthetic aperture radar: The 1997 eruption of Okmok volcano, Alaska," *IEEE Trans. Geosci. Remote Sens.*, vol. 41, no. 6, pp. 1428–1436, Jun. 2003.
[12] K. Dai, G. Liu, Z. Li, T. Li, B. Yu, X. Wang, and A. Singleton, "Extracting vertical displacement rates in Shanghai (China) with multi-platform SAR images," *Remote Sens.*, vol. 7, no. 8, pp. 9542–9562, 2015.
[13] Q. Huang, M. Crosetto, O. Monserrat, and B. Crippa, "Displacement monitoring and modelling of a high-speed railway bridge using C-band sentinel-1 data," *ISPRS J. Photogramm. Remote Sens.*, vol. 128, pp. 204–211, Jun. 2017.
[14] F. Chen, H. Guo, P. Ma, H. Lin, C. Wang, N. Ishwaran, and P. Hang, "Radar interferometry offers new insights into threats to the Angkor site," *Sci. Adv.*, vol. 3, no. 3, 2017, Art. no. e1601284.
[15] H. Fan, X. Gao, J. Yang, K. Deng, and Y. Yu, "Monitoring mining subsidence using a combination of phase-stacking and offset-tracking methods," *Remote Sens.*, vol. 7, no. 7, pp. 9166–9183, 2015.
[16] H. D. Fan, D. Cheng, K. Z. Deng, B. Q. Chen, and C. G. Zhu, "Subsidence monitoring using D-InSAR and probability integral prediction modelling in deep mining areas," *Surv. Rev.*, vol. 47, no. 345, pp. 438–445, 2015.
[17] S. Usai and R. Hanssen, "Long time scale InSAR by means of high coherence features," in *Proc. ERS Symp.*, vol. 414, 1997, pp. 225–228.
[18] S. Usai, *A New Approach for Longterm Monitoring of Deformations by Differential SAR Interferometry*. Delft, The Netherlands: Delft Univ. Press, 2001.
[19] S. Usai, "A least squares database approach for SAR interferometric data," *IEEE Trans. Geosci. Remote Sens.*, vol. 41, no. 4, pp. 753–760, Apr. 2003.
[20] A. Ferretti, C. Prati, and F. Rocca, "Nonlinear subsidence rate estimation using permanent scatterers in differential SAR interferometry," *IEEE Trans. Geosci. Remote Sens.*, vol. 38, no. 5, pp. 2202–2212, Sep. 2000.
[21] A. Ferretti, C. Prati, and A. Rocca, "Permanent scatterers in SAR interferometry," *IEEE Trans. Geosci. Remote Sens.*, vol. 39, no. 1, pp. 8–20, Jan. 2001.
[22] C. Werner, U. Wegmuller, T. Strozzi, and A. Wiesmann, "Interferometric point target analysis for deformation mapping," in *Proc. IEEE Int. Geosci. Remote Sens. Symp.*, Jul. 2003, pp. 4362–4364.
[23] P. Blanco-Sánchez, J. J. Mallorquí, S. Duque, and D. Monells, "The coherent pixels technique (CPT): An advanced DInSAR technique for nonlinear deformation monitoring," *Pure Appl. Geophys.*, vol. 165, no. 6, pp. 1167–1193, Aug. 2008.
[24] P. Berardino, G. Fornaro, R. Lanari, and E. Sansosti, "A new algorithm for surface deformation monitoring based on small baseline differential SAR interferograms," *IEEE Trans. Geosci. Remote Sens.*, vol. 40, no. 11, pp. 2375–2383, Nov. 2002.
[25] L. Zhang, X. Ding, and Z. Lu, "Ground settlement monitoring based on temporarily coherent points between two SAR acquisitions," *ISPRS J. Photogramm. Remote Sens.*, vol. 66, no. 1, pp. 146–152, 2011.
[26] L. Zhang, Z. Lu, X. Ding, H.-S. Jung, G. Feng, and C.-W. Lee, "Mapping ground surface deformation using temporarily coherent point SAR interferometry: Application to Los Angeles Basin," *Remote Sens. Environ.*, vol. 117, pp. 429–439, Feb. 2012.
[27] A. Hooper, "A multi-temporal InSAR method incorporating both persistent scatterer and small baseline approaches," *Geophys. Res. Lett.*, vol. 35, no. 16, pp. 96–106, 2008.
[28] T. G. Farr, P. A. Rosen, E. Caro, R. Crippen, R. Duren, S. Hensley, M. Kobrick, M. Paller, E. Rodriguez, L. Roth, D. Seal, S. Shaffer, J. Shimada, J. Umland, M. Werner, M. Oskin, D. Burbank, and D. Alsdorf, "The shuttle radar topography mission," *Rev. Geophys.*, vol. 45, no. 2, p. 361, 1998.
[29] A. Hooper, P. Segall, and H. Zebker, "Persistent scatterer interferometric synthetic aperture radar for crustal deformation analysis, with application to Volcán Alcedo, Galápagos," *J. Geophys. Res.*, vol. 112, no. B7, 2007, Art. no. B07407.
[30] A. Hooper and H. A. Zebker, "Phase unwrapping in three dimensions with application to InSAR time series," *J. Opt. Soc. Amer. A, Opt. Image Sci.*, vol. 24, no. 9, pp. 2737–2747, 2007.
[31] L. Peixian, "Study on regularity and prediction method of surface subsidence due to deep mining—Taking Xuzhou coal mining area as example," Ph.D. dissertation, China Univ. Mining Technol., Xuzhou, China, 2012.
[32] H. Weiyue, Z. Jianjun, and Y. Lanying, "Study on environment and safety disasters from abandoned coal mines," *J. Xi'An Univ. Sci. Technol.*, vol. 30, no. 4, pp. 436–440, 2010.
[33] Ö. Aydan and T. Ito, "The effect of the depth and groundwater on the formation of sinkholes or ground subsidence associated with abandoned room and pillar lignite mines under static and dynamic conditions," in *Proc. Int. Assoc. Hydrolog. Sci.*, vol. 372, 2015, pp. 281–284.
[34] A. Vervoort and P.-Y. Declercq, "Surface movement above old coal longwalls after mine closure," *Int. J. Mining Sci. Technol.*, vol. 27, no. 3, pp. 481–490, 2017.
[35] R. F. Bekendam and J. J. Pottgens, "Ground movements over the coal mines of southern Limburg, The Netherlands, and their relation to rising mine waters," *Int. J. Rock Mech. Min. Geomech. Abstr.*, vol. 33, no. 8, p. A377, 1996.
[36] G. Ren, J. Buckeridge, and J. Li, "Estimating land subsidence induced by groundwater extraction in unconfined aquifers using an influence function method," *J. Water Resour. Planning Manage.*, vol. 141, no. 7, 2015, Art. no. 04014084.
[37] K. Deng, Z. Tan, Y. Jiang, H. Dai, Y. Shi, and L. Xu, *Deformation Monitoring and Subsidence Engineering*. Xuzhou, China: China Univ. of Mining and Technology Press, 2014.
[38] T. Wanbing, C. Yurong, W. Fengmin, and Z. Xinkun, "Practical measure research on relationship between maximum subsidence value and coefficient of mining degree coefficient in deep mining," *Coal Technol.*, vol. 37, no. 11, pp. 49–51, 2018.
[39] Z. Hao, "Monitoring surface deformation of closed mine with an improved time-series InSAR technology," M.S. thesis, China Univ. Mining Technol., Xuzhou, China, 2018.
[40] *Geological Report of Jiahe Mine*, Xuzhou Great Wall Found. Eng., Xuzhou Mining Group, Xuzhou, China, 2012.
[41] *Geological Report of Zhang Xiaolou Mine*, Xuzhou Mining Group, Xuzhou, China, 2014.
[42] W. Milczarek, J. Blachowski, and P. Grzempowski, "Application of PSInSAR for assessment of surface deformations in post-mining area—Case study of the former Walbrzych hard coal basin (SW Poland)," *Acta Geodynamica Geomaterialia*, vol. 4, no. 1, pp. 41–52, 2017.